LETTERS
https://doi.org/10.1038/s41564-020-00810-x

nature microbiology

Transcriptional regulator-induced phenotype screen reveals drug potentiators in *Mycobacterium tuberculosis*

Shuyi Ma[1,2], Robert Morrison[1], Samuel J. Hobbs[2], Vijay Soni[3,4], Jessica Farrow-Johnson[1,2], Andrew Frando[2,5], Neil Fleck[2,5], Christoph Grundner[2,5], Kyu Y. Rhee[3,4], Tige R. Rustad[2] and David R. Sherman[1,2]✉

Transposon-based strategies provide a powerful and unbiased way to study the bacterial stress response[1–8], but these approaches cannot fully capture the complexities of network-based behaviour. Here, we present a network-based genetic screening approach: the transcriptional regulator-induced phenotype (TRIP) screen, which we used to identify previously uncharacterized network adaptations of *Mycobacterium tuberculosis* to the first-line anti-tuberculosis drug isoniazid (INH). We found regulators that alter INH susceptibility when induced, several of which could not be identified by standard gene disruption approaches. We then focused on a specific regulator, *mce3R*, which potentiated INH activity when induced. We compared *mce3R*-regulated genes with baseline INH transcriptional responses and implicated the gene *ctpD* (Rv1469) as a putative INH effector. Evaluating a *ctpD* disruption mutant demonstrated a previously unknown role for this gene in INH susceptibility. Integrating TRIP screening with network information can uncover sophisticated molecular response programs.

Deciphering the molecular stress response is important to studies of microbes, including *Mycobacterium tuberculosis*, the causative pathogen of tuberculosis[9]. Prolonged therapy and unfavourable outcomes arise partially because *M. tuberculosis* can persist in otherwise inhibitory drug concentrations by means independent of heritable resistance mutations[10–12]. Defining these adaptations can reveal biology, including unexplored drug targets and treatment-enhancing strategies. Screens of transposon-mediated gene disruption mutant pools[1–8] are powerful tools to identify candidate effector genes, but they also pose limitations: (1) they cannot identify genes whose upregulation elicits a phenotype; (2) essential genes are lost from experiments; and (3) they miss phenotypes from the coordinated actions of multiple genes. To address these limitations, we developed the transcriptional regulator-induced phenotype (TRIP) screen, which quantifies growth associated with individually inducing each *M. tuberculosis* transcription factor. TRIP offers several advantages: (1) emergent phenotypes are accessible, since regulons generally include multiple genes selected for co-regulation by evolution; (2) revealed phenotypes can be deconstructed with the existing baseline regulatory network; (3) transcription factor expression is chemically triggered, enabling context-specific interrogation of perturbations; and (4) essential regulators and effector genes can be assessed. Thus, TRIP is highly complementary to gene disruption-based screening approaches.

TRIP exploits a library of 207 transcription factor induction (TFI) strains, representing 97% of the annotated *M. tuberculosis* regulators, each transformed with a plasmid carrying a transcription factor under the control of a chemically inducible promoter (Fig. 1). Each strain is engineered for conditional induction of a single transcription factor and expression of its associated regulon—the set of genes whose expression changes when that transcription factor is induced[13–15]. Chromatin immunoprecipitation sequencing and expression profiling of TFI strains under in vitro log-phase conditions revealed a baseline network of transcriptional impacts and DNA binding interactions triggered by each transcription factor[13–15].

Here, we pool the TFI library for simultaneous growth measurements (Fig. 1). The pool is exposed to a stress condition either with or without TFI. The proportion of each TFI strain in the pool is quantified by next-generation sequencing of a DNA segment unique to each strain. Sampling the pool over time generates simultaneous abundance curves for each TFI strain. The abundance fold change of each strain when induced versus uninduced identifies regulons with altered growth or survival.

First, we applied TRIP to *M. tuberculosis* log-phase growth in vitro to characterize network perturbations that alter baseline fitness. Figure 2a visualizes the abundance fold change of each TFI strain when induced under these conditions (Supplementary Table 1 presents detailed results and individual replicate data). Most TFI strains showed no significant abundance difference upon induction (Fig. 2b shows an example TFI strain in this category). Twenty-two TFI strains (10.6%; below the dotted line at −0.5 in Fig. 2a) exhibited a growth defect upon TFI (Fig. 2c shows an example TFI strain in this category).

Growth-defective strains are enriched in transcription factors that activate genes associated with starvation responses (Supplementary Table 2). Such strains are also enriched for transcription factors that repress essential genes ($P < 10^{-6}$; hypergeometric test), although two defect-inducing TFIs (Rv3765c and Rv1255c) do not repress any essential genes, and 20 TFIs with no discernible growth phenotype do repress essential genes[3]. There is no significant correlation between the number of repressed essential genes and the extent of

[1]Department of Microbiology, University of Washington, Seattle, WA, USA. [2]Interdisciplinary Program of Pathobiology, Department of Global Health, University of Washington, Seattle, WA, USA. [3]Division of Infectious Diseases, Department of Medicine, Weill Cornell Medical College, New York, NY, USA. [4]Department of Microbiology and Immunology, Weill Cornell Medical College, New York, NY, USA. [5]Center for Global Infectious Disease Research, Seattle Children's Research Institute, Seattle, WA, USA. ✉e-mail: dsherman@uw.edu

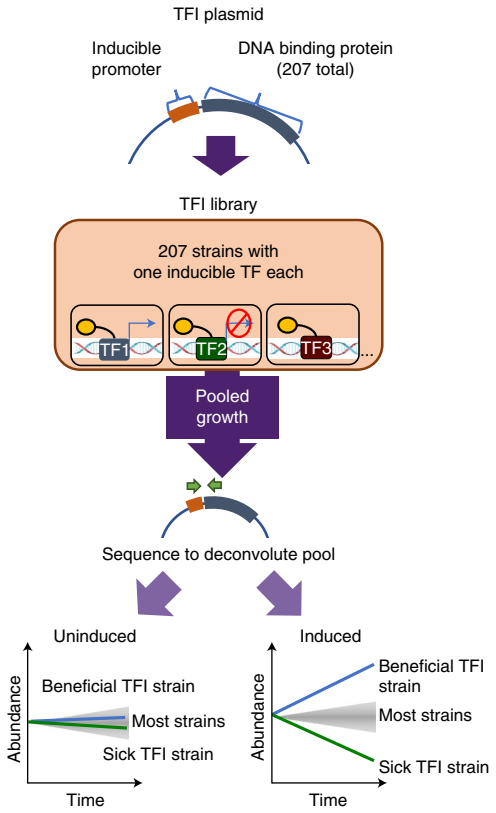

Fig. 1 | Schematic of the TRIP screen. See Methods for details. TF, transcription factor.

growth defect incurred by the TFI strain, which could potentially arise for several reasons, including synthetic rescues[16,17] or the non-linear relationship between expression level and fitness for some essential genes[18].

To validate relative abundance differences detected by TRIP, we compared screening results with the growth of each individual TFI strain over a 1-week time course with and without TFI. Of the 22 TFIs with a strong growth defect in TRIP, 20 also had a strong growth defect when cultured individually. Out of 174 other transcription factors with no TRIP-associated defect, only one TFI strain elicited a greater than 1.5-fold increase in doubling time when transcription factor expression was induced in monoculture. Notably, these 174 TFI strains included 23 transcription factors that we had previously characterized to elicit no transcriptional change when induced under log-phase growing conditions. These validations indicate that: (1) phenotypes detected by TRIP reflect growth observed in monoculture; (2) significant growth defect upon TFI is uncommon and transcription factor specific; and (3) protein (and transcription factor) overexpression do not convey non-specific growth defects.

With baseline *M. tuberculosis* network phenotypes established, we applied TRIP to study responses to the frontline anti-tuberculosis agent isoniazid (INH). We exposed TFI pools to an INH dose where the bulk population grew suboptimally (19% of untreated; Extended Data Fig. 1), enabling the identification of TFIs with either reduced or improved viability compared with the population average from a single experiment. Figure 2d shows the abundance of TFI strains exposed to drug when induced relative to uninduced. Strains with significant INH phenotypes partition into three groups: (1) TFIs conveying a growth advantage in INH but no change when untreated (six strains; purple box; group 1); (2) TFIs conveying a growth defect in INH but no change when untreated (four strains; dark blue box; group 2); and (3) TFIs conveying a growth defect in INH and untreated conditions (nine strains; light blue box; group 3). Of the 20 transcription factors that yield INH TRIP phenotypes, two were revealed by transposon insertion sequencing (Tn-seq) to alter *M. tuberculosis* fitness significantly during INH treatment (Supplementary Table 2)[19]. The regulons of transcription factors in all three groups were enriched for genes reported to alter INH fitness by Tn-seq (Supplementary Table 3)[19]. Notably, two of the four transcription factors in group B solely activate genes when induced (Rv0330c and Rv2282c), so association between genes in these regulons and INH fitness could not have been detected by disruption-based assays.

The TFI conveying the greatest TRIP advantage in INH is *furA* (Rv1909c). This transcription factor represses the expression of *katG* (Rv1908c), which encodes the catalase–peroxidase that converts the INH prodrug into its active form[20,21]. Inducing *furA* is known to restore nearly uninhibited growth in INH[14,20,22].

Next, we investigated regulons representing potential therapeutic targets. The transcription factor conveying the greatest INH TRIP defect is *mce3R* (Rv1963c)—a TetR-like regulator. *mce3R* has been linked to the expression of genes that mediate β-oxidation of fatty acids and lipid transport[23–25] and had no previous connection to INH.

To validate hypersusceptibility, we tested the viability of the *mce3R* induction strain ($mce3R_{ind}$) in monoculture with INH. First, we exposed $mce3R_{ind}$ to INH, with and without TFI (Fig. 2e). We confirmed *mce3R* induction by quantitative PCR (qPCR) (Extended Data Fig. 2) and observed a significant, fourfold additional survival defect by 7 d of INH. By day 14, during the *M. tuberculosis* growth rebound phase mediated by INH degradation in the culture media[26–28], the additional *mce3R* defect was 21-fold. We suspect that this is because many common *katG* mutations still retain some catalase activity and INH sensitivity[29], although we have not precluded other possible explanations. We also assayed *M. tuberculosis* ATP levels (BacTiter-Glo; Promega) after 7 d with varying INH doses (Fig. 2f and Extended Data Fig. 3). We found that, at every non-zero INH concentration tested, *mce3R* induction resulted in significantly lower metabolic viability, demonstrating that *mce3R*-mediated hypersusceptibility is independent of drug dose.

Hypersusceptibility could stem from TFI-mediated countering of the *M. tuberculosis* adaptation to INH. To investigate this hypothesis, we compared the *mce3R* induction regulon from our basal transcriptional network with genes previously shown to be differentially expressed when H37Rv is exposed to INH[14,30,31]. *ctpD* (Rv1469) is one of two genes repressed by *mce3R* (Fig. 3a; see Extended Data Fig. 4 for the full set) and is normally upregulated in response to INH in broth culture and under macrophage infection conditions[30,31]. After excluding the other gene (see Supplementary Tables 4 and 5 for details), we hypothesized that *ctpD* induction might be important for temporary *M. tuberculosis* adaptation to INH. If so, depleting *ctpD* might elicit INH hypersusceptiblity independent from *mce3R*.

To test whether *ctpD* influences INH susceptibility, we obtained a transposon mutant that disrupted *ctpD* (*ctpD*::Himar1). We compared kill curves for *ctpD*::Himar1 versus the parent strain CDC1551 when exposed to INH (Fig. 3b and Extended Data Fig. 5). As predicted, *ctpD*::Himar1 survival was reduced relative to CDC1551 following INH (93-fold difference after 7 d; $P = \sim 3 \times 10^{-5}$; *t*-test), with no significant growth difference without the drug. To independently validate this INH hypersusceptibility, we performed a CRISPR interference (CRISPRi)-mediated knockdown of *ctpD* in H37Rv. Without anhydrotetracycline (ATc), *ctpD* expression in the CRISPRi strain is 15% of H37Rv, and it exhibits a 95-fold colony-forming unit (c.f.u.) reduction relative to H37Rv at 7 d of INH. With ATc supplementation, *ctpD* expression in the CRISPRi

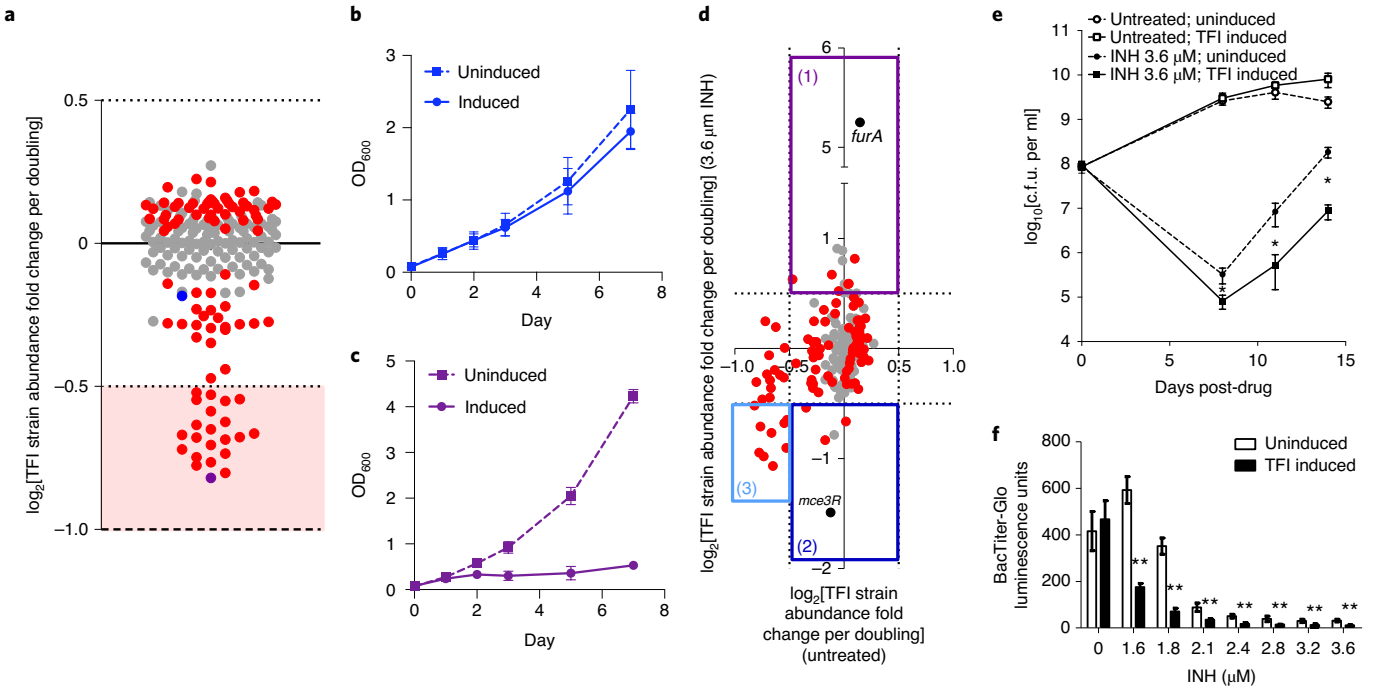

Fig. 2 | Regulon-mediated growth responses. a, Log-phase TRIP results for untreated strains. The dots represent the mean abundance change of induced versus uninduced TFI strains, normalized by the estimated number of pool doublings (averaged from four biological replicates). Red dots indicate a *z* score > 1, calculated from four replicates. The dotted lines specify ±2 s.d. and the dashed line denotes the detection limit, signifying no growth. The shaded area represents strains with strong defects. The blue and purple dots indicate the strains shown in **b** and **c**, respectively. **b**,**c**, Monoculture growth curves of two strains (blue (**b**) and purple dots (**c**) from **a**), with (solid) or without induction (dashed). Means ± s.d. of three biological replicates from three independent experiments are shown. **d**, TRIP results with 3.6 μm INH (*y* axis) versus no drug (*x* axis). Each dot represents a mean of four biological replicates. Since INH can be bactericidal, some strains showed abundance changes < −1. The boxes demarcate strains with altered INH survival: (1) TFIs conveying a growth advantage in INH but no change when untreated (six strains; purple box); (2) TFIs conveying a growth defect in INH but no change when untreated (four strains; dark blue box); and (3) TFIs conveying a growth defect in INH and untreated conditions (nine strains; light blue box). The black dots represent strains: *furA* ($furA_{ind}$) and *mce3R* ($mce3R_{ind}$). **e**, $mce3R_{ind}$ c.f.u. per ml over 14 d in INH (filled points) versus no drug (open points), with (solid lines) or without induction (dashed lines). Means ± s.d. of three biological replicates from one representative experiment are shown (the experiment was performed independently three times). *P* values were as follows: $^{*}P = 0.00012$ (uninduced versus TFI induced in INH on day 8); $^{*}P = 0.015$ (uninduced versus TFI induced in INH on day 11); and $P = 7.0 \times 10^{-8}$ (uninduced versus TFI induced in INH on day 14). **f**, $mce3R_{ind}$ metabolic viability after 7 d INH with (black) or without induction (white), measured by luminescence (see Methods). Means ± s.d. of four biological replicates from one representative experiment are shown (the experiment was performed independently three times). See Extended Data Fig. 3 for a version of **f** with the individual replicates visualized and the exact *P* values for each individual comparison enumerated. Asterisks in **e** and **f** indicate significant differences between induction states ($^{*}P < 0.05$; $^{**}P < 0.001$; two-sided *t*-test in all instances).

strain is 8% of H37Rv and it exhibits a 275-fold c.f.u. reduction relative to H37Rv at 7 d of INH (Extended Data Fig. 5; see Methods for CRISPRi details). We also found that inducing *mce3R* expression in the *ctpD*::Himar1 strain conveyed a greater c.f.u. decrease at 7 d of INH treatment than the *ctpD*::Himar1 strain alone (Extended Data Fig. 6). This suggests that additional components of the *mce3R* regulon also contribute to INH sensitivity. Transcriptome profiling[14] revealed no significant expression change in the thioredoxin genes *trxA* (Rv1470) and *trxB1* (Rv1471) upon *mce3R* induction ($P > 0.3$; *t*-test), suggesting that polar effects on the genes downstream of *ctpD* are unlikely to contribute significantly to the INH susceptibility phenotype.

The *ctpD* gene encodes a membrane protein[32] annotated as the *M. tuberculosis* paralogue of CtpD—a member of the metal cation-transporting P1B4-ATPase subgroup—and is essential for *M. tuberculosis* survival in the host[2,33,34]. CtpD is a high-affinity Fe^{2+} exporter needed to overcome redox stress and adapt to the host[33,35]. Given that KatG-mediated catalysis is iron dependent, Fe^{2+} accumulation from *ctpD* loss could possibly increase levels of oxy-ferrous KatG, which in turn could increase INH activation[36]. Consistent with this hypothesis, metabolic profiling of the *ctpD*::Himar1 and $mce3R_{ind}$ strains showed increased intracellular accumulation of INH and activated INH-NAD adduct[37] (Fig. 3c and Extended Data Fig. 7). Notably, *mce3R* induction in *ctpD*::Himar1 does not convey additional INH-NAD adduct accumulation, suggesting that *ctpD* is a major contributor of *mce3R*-mediated modulation of INH activation. Alternatively, extra free iron in *M. tuberculosis* could promote cell wall changes[19] or increased oxidative stress[38] that may enhance INH activity. RNA sequencing (RNA-seq) transcriptome profiling of the *ctpD*::Himar1 strain indicated that *katG* expression was ~1.7-fold higher and *furA* expression was ~2.1 fold higher than the wild type after 1 d of INH ($P < 0.01$; *t*-test). Given the aforementioned link between *furA* and *katG*[14,20,22], it is possible that the *ctpD*-mediated phenotype is partially mediated by a change in *katG* expression. Further work is needed to establish the mechanism of CtpD-mediated intrinsic INH susceptibility, and whether this mechanism extends to other cation transmembrane transporters.

TRIP represents a powerful tool to unravel the links between genetic perturbations and their phenotypic outcomes under various environmental contexts. Previous transcription factor-centric strat-

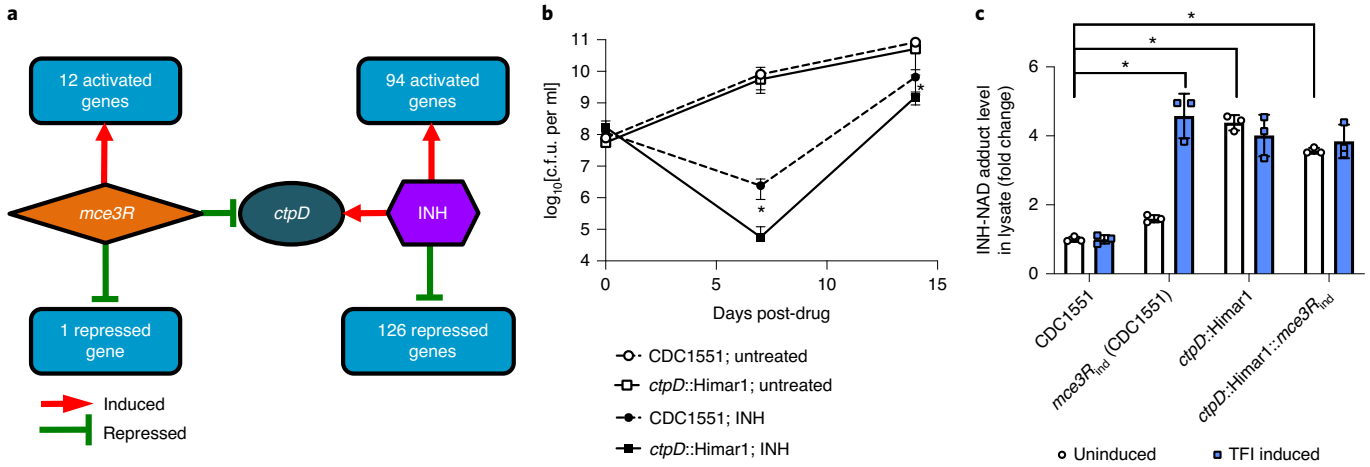

Fig. 3 | *mce3R* regulon reveals effector of INH susceptibility. a, Network representation of the overlap between the *mce3R* regulon and genes differentially expressed in the wild-type response to INH exposure. Red arrows indicate genes activated at least twofold. Green lines indicate genes repressed at least twofold. **b**, c.f.u. per ml over 14 d of the *ctpD*::Himar1 transposon disruption strain (solid lines) compared with the wild-type strain, CDC1551 (dashed lines). Both strains were exposed to 3.6 μM INH (filled points) versus no drug (open points). Means ± s.d. from three biological replicates of one representative experiment are shown (the experiment was performed independently three times). *P* values, as determined by two-sided *t*-test, were as follows: **P* = 0.0021 (CDC1551 + INH on day 7 versus *ctpD*::Himar1 + INH on day 7); and **P* = 0.029 (CDC1551 + INH on day 14 versus *ctpD*::Himar1 + INH on day 14). **c**, Mass spectrometry quantification of relative intracellular INH-NAD adduct levels in the $mce3R_{ind}$ and *ctpD*::Himar1 strains after 24 h of exposure to 7.2 μM INH. Elevated INH-NAD levels are seen relative to the wild type. There was no significant difference between INH-NAD levels in the *ctpD*::Himar1 strain with and without *mce3R* induction. Means ± s.d. of three biological replicates from one representative experiment are shown (the experiment was performed independently twice). *P* values, as determined by two-sided *t*-test, were as follows: **P* = 0.00067 (CDC1551 versus $mce3R_{ind}$ (CDC1551) TFI induced); **P* = 0.000015 (CDC1551 versus *ctpD*::Himar1); **P* = 0.00057 (CDC1551 versus *ctpD*::Himar1::$mce3R_{ind}$ TFI induced); and **P* = 0.16 (*ctpD*::Himar1 versus *ctpD*::Himar1::$mce3R_{ind}$ TFI induced).

egies profiled individual transcription factor perturbation strains separately, requiring up to hundreds of cultures to capture regulatory fitness in a single condition[14,31,39,40]. In contrast, TRIP enables parallelized fitness quantification across *M. tuberculosis* transcription factors within a single culture. TRIP can reveal associations between genes, networks and fitness in several ways. First, by targeting regulons, TRIP harnesses nature's levers to modulate responses—tuning gene sets that evolved to change coordinately—and uncovers phenotypes that depend on synchronized actions of multiple genes. For example, two TFIs that slowed growth under log-phase conditions (Rv3765c and Rv1255c) do not repress any essential genes, suggesting that epistatic mechanisms may underlie these defects. Second, TRIP samples network states distinct from those elicited by transcription factor disruption. For example, *mce3R* was previously reported to regulate the *mce3* operon genes based on studies of a deletion mutant[23,24]. However, the transcriptional impact of inducing *mce3R* does not include the *mce3* operon (Supplementary Table 2 shows the full regulon, based on ref. [14]), suggesting that *mce3R* participates in complex regulatory circuits. Combining gene disruption studies with TRIP and network analysis could facilitate deconstructing these nonlinear effects. Finally, unlike gene disruption assays, TRIP can profile upregulation phenotypes, as with the INH hypersusceptibility-inducing transcription factors Rv0330c and Rv2282c, both of which exclusively activate genes.

In this study, we combined TRIP with network analysis to identify genes that altered the *M. tuberculosis* response to INH. However, TRIP can interrogate network mediators of fitness under any condition from which microbes can be recovered, and TRIP requires tracking a substantially reduced set of mutants compared with Tn-seq, rendering it technically tractable. By integrating with network information, TRIP will lend insights into emergent mechanisms underlying condition-specific growth phenotypes in *M. tuberculosis*, and the strategy can be generalized for other organisms.

Methods

Strains and expression vectors. The individual strains comprising the *M. tuberculosis* TFI library were generated previously[14]. Briefly, 207 *M. tuberculosis* DNA binding genes were cloned into a tagged, inducible vector that placed the transcription factor under control of a tetracycline-inducible promoter and added a carboxy-terminal FLAG epitope tag[14,41–44]. The constructs were then individually transformed into *M. tuberculosis* H37Rv using standard methods. Individual TFI strains are available from the BEI strain repository of the American Type Culture Collection[45]. The TFI library was generated by combining equal proportions of each strain into a common pool.

The *ctpD* transposon strain (*ctpD*::Himar1) was obtained through BEI Resources, National Institute of Allergy and Infectious Diseases, National Institutes of Health: *M. tuberculosis*: Strain CDC1551, Transposon Mutant 1738 (MT1515, Rv1469), NR-18218 (ref. [45]). The transposon insertion is located at base 671 in the 1,974-base-pair-long gene[45]. To trigger *mce3R* induction in this strain, we transformed the *mce3R* TFI plasmid into *ctpD*::Himar1, to generate the *ctpD*::Himar1::$mce3R_{ind}$ strain. As an additional control, we also generated an $mce3R_{ind}$ (CDC1551) strain by transforming the *mce3R* TFI plasmid into the CDC1551 strain background.

The *ctpD* CRISPRi strain was constructed according to the method outlined previously[46]. Briefly, we used the pJR965 plasmid encoding a tetracycline-inducible dCas9, a tetracycline-inducible *ctpD*-specific single guide RNA (sgRNA) and a kanamycin-selectable marker. We made the *ctpD*-specific sgRNA by annealing two complementary oligonucleotides targeting the non-template strand of the *ctpD* open reading frame 3′ of a protospacer-adjacent motif sequence (forward primer sequence: GGGAGTTCAGTTGCGCCACTAGTCCGG; reverse primer sequence: AAACCCGGACTAGTGGCGCAACTGAAC). pJR965 was digested with BsmBI, and *ctpD*-specific sgRNA was ligated into digested pJR965 using T4 DNA ligase. The ligation reaction was transformed into competent *Escherichia coli* and sgRNA insertions were confirmed by Sanger sequencing before the plasmids were transformed into *M. tuberculosis*.

Culture. Bacteria were cultured at 37 °C under aerobic conditions with constant agitation. For the experiments involving TFI strains, the strains were cultured in Middlebrook 7H9 supplemented with albumin dextrose catalase (Difco), 0.05% Tween 80 and 50 μg ml^{-1} hygromycin B to maintain the plasmids.

For the TRIP experiments, growth of the pooled TFI library was monitored by measuring the optical density measured at a wavelength of 600 nm (OD_{600}). At an OD_{600} of 0.1, expression of the pooled TFI library was induced with ATc

(100 ng ml^{-1}) and the cultures were grown for 7 d supplemented with either 3.6 µM INH in 1% dimethyl sulfoxide (DMSO) solution or DMSO as a no-drug control. The cultures were sampled at days 0 and 7 of the experiment for DNA isolation and subsequent sequencing.

For individual TFI strain time-course experiments, each strain was cultured under the same media conditions as described for the pooled TFI library. When cultures reached an OD_{600} of ~0.1, TFI strain induction and drug exposure proceeded as described for the pooled TFI library. The individual strain cultures were monitored for up to 14 d, with viability under the different drug and induction conditions assayed by plating on Middlebrook 7H10 solid media plates and assessing the c.f.u. using standard methods.

The *ctpD*::Himar1 strain was cultured in Middlebrook 7H9 supplemented with albumin dextrose catalase (Difco), 0.05% Tween 80 and 30 µg ml^{-1} kanamycin to maintain the transposon insertion. The growth and survival of the Rv1469 mutant were compared against the parent *M. tuberculosis* CDC1551 strain. When cultures reached an OD_{600} of 0.1, drug exposure proceeded as described for the pooled TFI library. The individual strain cultures were monitored for up to 14 d, with viability under the different drug and induction conditions assayed by plating on Middlebrook 7H10 solid media plates and assessing the c.f.u. using standard methods.

To prepare for metabolomics profiling, *M. tuberculosis* strains were cultured at 37 °C in Middlebrook 7H9 broth (BD) containing 0.2% glycerol, 0.04% Tyloxapol, 0.85 g l^{-1} NaCl, 2 g l^{-1} D-glucose and 5 g l^{-1} Fraction V BSA (Roche).

Dose-dependent viability assay. Strains were grown to the log phase (OD_{600} = ~0.3), diluted to a final OD_{600} of 0.005 and dispensed into 96-well flat-bottom plates (Corning) at a final volume of 200 µl, containing 1% DMSO and varying concentrations of INH in the different wells. On each plate, control wells for each of the strains studied were included, containing no drug and 1% DMSO vehicle, to measure the viability in the absence of INH exposure. The plates were incubated at 37 °C for 7 d. Cellular viability was assayed on day 7 by adding 20 µl culture from each well to 20 µl BacTiter-Glo Microbial Cell Viability Assay reagent (Promega), with incubation at room temperature under protection from direct light for 20 min, and reading the luminescence intensity using a FLUOstar Omega plate reader (BMG Labtech).

DNA isolation and sequencing. Cell pellets collected from each sample were resuspended in Tris-EDTA buffer (pH 8.0), transferred to a tube containing Lysing Matrix B (Qbiogene) and vigorously shaken three times at 6 m s^{-1} for 30 s per cycle in a Bead Ruptor 24 homogenizer (Omni International), with a 30-s pause between each cycle. The mixture was centrifuged at maximum speed for 1 min and DNA was extracted from the supernatant using the MagJET Genomic DNA Kit (Thermo Fisher Scientific), according to the manufacturer's instructions for manual genomic DNA purification.

PCR pre-amplification of DNA barcodes unique to each TFI strain was performed. The products of this reaction were prepared for Illumina sequencing using the NEBNext Ultra DNA Library Prep Kit for Illumina (New England Biolabs) according to the manufacturer's instructions, and using the AMPure XP reagent (Agencourt Bioscience Corporation) for size selection and cleanup of adaptor-ligated DNA. We used the NEBNext Multiplex Oligos for Illumina (Dual Index Primers Set 1) to barcode the DNA libraries associated with each replicate and enable multiplexing of 96 libraries per sequencing run. The prepared libraries were quantified using the Kapa qPCR quantification kit and sequenced at the University of Washington Northwest Genomics Center with the Illumina NextSeq 500 Mid Output v2 Kit (Illumina). The sequencing generated an average of 1.5 million 75-base pair paired-end raw read counts per library.

Sequencing read alignment and TFI strain abundance deconvolution. Read alignment was carried out using a custom processing pipeline that harnesses the Bowtie 2 utilities[47,48], which is available at https://github.com/DavidRShermanLab/TRIPscreen, https://github.com/robertdouglasmorrison/DuffyNGS and https://github.com/robertdouglasmorrison/DuffyTools (ref. [49]). A custom Bowtie 2 target index was constructed from: the CDS sequences of all H37Rv genes; the inducible TFI anchor plasmid sequence; and the complete sequence of the empty plasmid as a negative control. The two mate-pair FASTQ datasets for each sample were separately mapped as unpaired reads using the local alignment mode of Bowtie 2. After both mate-pair datasets were aligned separately, the alignment results were combined to give a pair of gene/plasmid alignments for each raw read. Only raw read pairs having one alignment to the anchor plasmid and the other to a gene with an existing Rv code were kept as valid reads. Read pairs that mapped to Rv code genes on both ends, or pairs that failed to align, were discarded. On average, each sample had 99.9% valid anchor/gene reads, which is comparable to typical RNA-seq and whole-genome sequencing alignment results. Libraries that generated fewer than 10,000 valid read pairs were excluded from further analysis. Valid reads were then tallied for all Rv code genes reported as raw abundance measures. Read counts for each TFI were then normalized as $\log_2$[reads per million (RPM)] values. Higher RPM values indicated that the corresponding TFI strain had greater relative abundance in the pooled culture. The average $\log_2$[RPM] value across TFIs was 11.7 ± 3.2. TFIs with low abundance levels on day 0 of each experiment ($\log_2$[RPM] < 5) were excluded from subsequent analysis (ten TFI strains; 4.8%).

We performed each TRIP experiment on two independent occasions, and included four biological replicates per condition on each occasion. To assess the effect of induction on TFI strain relative abundance, the $\log_2$[fold-change RPM] values of each replicate were calculated for the TFI-induced condition relative to the uninduced condition. These values were averaged and further normalized by the number of doublings of the pooled library estimated from the change in OD_{600} over the course of the experiment. Positive fold-change RPM values indicated that TFI induction conveyed a growth benefit, whereas negative fold-change RPM values indicated that the TFI induction conveyed a growth defect under the conditions assayed. We estimated the statistical significance of the TFI-mediated $\log_2$[fold-change abundance] values detected in two ways. For each TFI strain, we first calculated a *z* score for each TFI-induced replicate, relative to uninduced. This was intended to assess the number of standard deviations a particular TFI-induced replicate was away from the null distribution estimated from the uninduced replicates. We calculated the *z* score of the *i*th TFI-induced replicate using the following formula: $z_i = \frac{x_{+,i} - \overline{x_-}}{\sigma_-}$, where $x_{+,i}$ represents the $\log_2$[RPM] value for the *i*th TFI-induced replicate, $\overline{x_-}$ represents the average $\log_2$[RPM] value across uninduced TFI replicates, and σ_- represents the standard deviation of the $\log_2$[RPM] values across uninduced TFI replicates. We can then summarize the *z* score associated with a TFI by averaging the *z* scores calculated across induced TFI replicates. In addition to assessing significance by *z* score, we also calculated *P* values of $\log_2$[RPM fold change] associated with each TFI strain induction using the Student's *t*-test. TFI strains that exhibited a $\log_2$[fold change] per doubling greater than 0.5 with a *z* score greater than 1 and a *t*-test *P* value < 0.05 were deemed to have a significant growth phenotype under the condition assayed. The full *z* scores and *P* values for each TFI strain are reported in Supplementary Table 1. The code used to generate this processing is available at https://github.com/DavidRShermanLab/TRIPscreen.

RNA-seq transcriptome profile data generation. To profile the *M. tuberculosis* transcriptome response to exposure of individual drugs, cultures were diluted to an OD_{600} of ~0.2 (equivalent to 10^8 c.f.u. per ml) and exposed to a minimum inhibitory concentration-equivalent dose of drug for approximately 16 h.

RNA was isolated from these cultures and prepared for sequencing as described previously[14,49,50]. Briefly, cell pellets in TRIzol were transferred to a tube containing Lysing Matrix B (Qbiogene) and vigorously shaken at maximum speed for 30 s in a FastPrep FP120 homogenizer (Qbiogene) three times, with cooling on ice between shakes. This mixture was centrifuged at maximum speed for 1 min and the supernatant was transferred to a tube containing 300 µl chloroform and Heavy Phase Lock Gel (Eppendorf). This tube was inverted for 2 min and centrifuged at maximum speed for 5 min. RNA in the aqueous phase was then precipitated with 300 µl isopropanol and 300 µl high salt solution (0.8 M sodium citrate and 1.2 M NaCl). RNA was purified using an RNeasy kit following the manufacturer's recommendations (Qiagen) with one on-column DNase treatment (Qiagen). The total RNA yield was quantified using a NanoDrop (Thermo Scientific).

To enrich the messenger RNA, ribosomal RNA was depleted from samples using the Ribo-Zero rRNA removal (bacteria) magnetic kit (Illumina). The products of this reaction were prepared for Illumina sequencing using the NEBNext Ultra RNA Library Prep Kit for Illumina (New England Biolabs) according to the manufacturer's instructions, and using the AMPure XP reagent (Agencourt Bioscience Corporation) for size selection and cleanup of adaptor-ligated DNA. We used the NEBNext Multiplex Oligos for Illumina (Dual Index Primers Set 1) to barcode the DNA libraries associated with each replicate. To achieve adequate sequencing coverage, we multiplexed 40 libraries per sequencing run. The prepared libraries were quantified using the KAPA qPCR quantification kit and were sequenced at the University of Washington Northwest Genomics Center with the Illumina NextSeq 500 High Output v2 Kit (Illumina). The sequencing generated an average of 75 million-base-pair single-end raw read counts per library.

Read alignment was carried out using the previously mentioned custom processing pipeline that harnesses the Bowtie 2 utilities[47,48], available at https://github.com/robertdouglasmorrison/DuffyNGS and https://github.com/robertdouglasmorrison/DuffyTools (ref. [49]). The RNA-seq data profiling response to drug exposure generated for this study are publicly available from the Gene Expression Omnibus at GSE151991.

Metabolite extraction. Metabolomics experiments and analysis were performed according to published literature[51]. One millilitre of mid-log-phase cultures (OD_{580} = 0.8–1) was passed through 0.22-µm nylon filters and allowed to grow at 37 °C for 5 d on Middlebrook 7H11 agar (BD) supplemented with 0.2% glycerol, 0.85 g l^{-1} NaCl, 2 g l^{-1} D-glucose and 5 g l^{-1} Fraction V BSA (Roche). On day 6, *M. tuberculosis*-laden filters were transferred onto a reservoir containing 7H9 media (without tyloxapol) with 50 ng ml^{-1} ATc and left at 37 °C for 24 h. Next, these acclimatized filters were exposed to fresh 7H9 media with and without INH (7.2 µM) and ATc. After 24 h, these filters were quenched in a precooled (−40 °C) mix of acetonitrile, methanol and water (40%:40%:20%). Metabolites were extracted by bead beating using 0.1 mm Zirconia beads and Precellys homogenizer

(Bertin Instruments). Lysates were centrifuged and decontaminated by passing through Spin-X tube filters (0.22 µm; Sigma–Aldrich).

Mass spectrometry and liquid chromatography. Metabolomics was performed by separating a 2 µl sample on a Diamond Hydride Type C Column (Cogent) using 1200 liquid chromatography (Agilent) coupled to an Agilent Accurate-Mass 6220 Time-of-Flight spectrometer. To collect all classes of metabolites, two different solvents (solvent A (water with 0.2% formic acid) and solvent B (acetonitrile with 0.2% formic acid)) were used at the following gradients with a flow rate of 0.4 ml min^{-1}: 85% B for 0–2 min; 80% B for 3–5 min; 75% B for 6–7 min; 70% B for 8–9 min; 50% B for 10–11 min; 20% B for 11–14 min; 5% B for 14–24 min and 10 min of re-equilibration period using 85% B. Ion abundances of INH and INH-NAD were determined using Profinder 8.0 and Qualitative Analysis 7.0 (Agilent Technologies). Standard INH and INH-NAD were used to determine the accuracy of the identified peaks. Fold changes were calculated with respect to the abundances of corresponding wild-type strains (H37Rv or CDC1551).

Statistics and reproducibility. Unless otherwise indicated, the experiments were performed three times and the mean and standard deviation from biological replicates of representative experiments are reported. Statistical differences between means were evaluated by two-tailed Student's *t*-test; statistically significant correlation was evaluated by calculating a Pearson correlation coefficient and comparing against a Student's *t*-distribution; and statistical enrichment was evaluated by hypergeometric test, unless otherwise noted. The significance cut-off was set at $P < 0.05$, unless otherwise indicated.

Gene Ontology enrichment analysis. The Gene Ontology term annotations for genes comprising the regulons of the transcription factors under analysis were taken from ref. [52] and evaluated for statistical enrichment against the Gene Ontology annotations for the entire gene set of the *M. tuberculosis* strain H37Rv using the hypergeometric test, then further subjected to a Bonferroni correction for multiple hypothesis testing, with the number of independent tests estimated as the number of Gene Ontology terms associated with at least two genes in the H37Rv reference gene set (analogous to the method used by ref. [53]). We further filtered the enriched Gene Ontology terms to only those featured in the regulons for two more of the transcription factors under analysis.

Reporting Summary. Further information on research design is available in the Nature Research Reporting Summary linked to this article.

Data availability

The data reported in this paper are available in Supplementary Tables 1–5. The raw TRIP fastq sequence data files are deposited in the Sequence Read Archive database under accession PRJNA483505. The RNA-seq data are deposited in the Gene Expression Omnibus database under accession GSE151991. The TFI strains are available from BEI Resources (https://www.beiresources.org/Home.aspx).

Code availability

The code required to process the TRIP and RNA-seq sequenced reads are available at https://github.com/robertdouglasmorrison/DuffyNGS, https://github.com/robertdouglasmorrison/DuffyTools and https://github.com/DavidRShermanLab/TRIPscreen.

Received: 1 May 2018; Accepted: 5 October 2020;
Published online: 16 November 2020

References

1. Sassetti, C. M., Boyd, D. H. & Rubin, E. J. Comprehensive identification of conditionally essential genes in mycobacteria. *Proc. Natl Acad. Sci. USA* **98**, 12712–12717 (2001).
2. Sassetti, C. M. & Rubin, E. J. Genetic requirements for mycobacterial survival during infection. *Proc. Natl Acad. Sci. USA* **100**, 12989–12994 (2003).
3. Griffin, J. E. et al. High-resolution phenotypic profiling defines genes essential for mycobacterial growth and cholesterol catabolism. *PLoS Pathog.* **7**, e1002251 (2011).
4. Langridge, G. C. et al. Simultaneous assay of every *Salmonella* Typhi gene using one million transposon mutants. *Genome Res.* **19**, 2308–2316 (2009).
5. Gallagher, L. A., Shendure, J. & Manoil, C. Genome-scale identification of resistance functions in *Pseudomonas aeruginosa* using Tn-seq. *mBio* **2**, e00315-10 (2011).
6. Van Opijnen, T., Bodi, K. L. & Camilli, A. Tn-seq: high-throughput parallel sequencing for fitness and genetic interaction studies in microorganisms. *Nat. Methods* **6**, 767–772 (2009).
7. Goodman, A. L. et al. Identifying genetic determinants needed to establish a human gut symbiont in its habitat. *Cell Host Microbe* **6**, 279–289 (2009).
8. Gawronski, J. D., Wong, S. M., Giannoukos, G., Ward, D. V. & Akerley, B. J. Tracking insertion mutants within libraries by deep sequencing and a genome-wide screen for *Haemophilus* genes required in the lung. *Proc. Natl Acad. Sci. USA* **106**, 16422–16427 (2009).
9. *Global Tuberculosis Report 2016* (World Health Organization, 2016).
10. Warner, D. F. & Mizrahi, V. Tuberculosis chemotherapy: the influence of bacillary stress and damage response pathways on drug efficacy. *Clin. Microbiol. Rev.* **19**, 558–570 (2006).
11. Aldridge, B. B., Keren, I. & Fortune, S. M. The spectrum of drug susceptibility in mycobacteria. *Microbiol. Spectr.* **2**, https://doi.org/10.1128/microbiolspec.MGM2-0031-2013 (2014).
12. Wallis, R. S. et al. Drug tolerance in *Mycobacterium tuberculosis*. *Antimicrob. Agents Chemother.* **43**, 2600–2606 (1999).
13. Minch, K. J. et al. The DNA-binding network of *Mycobacterium tuberculosis*. *Nat. Commun.* **6**, 5829 (2015).
14. Rustad, T. R. et al. Mapping and manipulating the *Mycobacterium tuberculosis* transcriptome using a transcription factor overexpression-derived regulatory network. *Genome Biol.* **15**, 502 (2014).
15. Galagan, J. E. et al. The *Mycobacterium tuberculosis* regulatory network and hypoxia. *Nature* **499**, 178–183 (2013).
16. Motter, A. E., Gulbahce, N., Almaas, E. & Barabasi, A. L. Predicting synthetic rescues in metabolic networks. *Mol. Syst. Biol.* **4**, 168 (2008).
17. Wytock, T. P. et al. Experimental evolution of diverse *Escherichia coli* metabolic mutants identifies genetic loci for convergent adaptation of growth rate. *PLoS Genet.* **14**, e1007284 (2018).
18. Wei, J. R. et al. Depletion of antibiotic targets has widely varying effects on growth. *Proc. Natl Acad. Sci. USA* **108**, 4176–4181 (2011).
19. Xu, W. et al. Chemical genetic interaction profiling reveals determinants of intrinsic antibiotic resistance in *Mycobacterium tuberculosis*. *Antimicrob. Agents Chemother.* **61**, e01334-17 (2017).
20. Pym, A. S. et al. Regulation of catalase–peroxidase (KatG) expression, isoniazid sensitivity and virulence by *furA* of *Mycobacterium tuberculosis*. *Mol. Microbiol.* **40**, 879–889 (2001).
21. Zahrt, T. C., Song, J., Siple, J. & Deretic, V. Mycobacterial FurA is a negative regulator of catalase–peroxidase gene *katG*. *Mol. Microbiol.* **39**, 1174–1185 (2001).
22. Zhang, Y., Heym, B., Allen, B., Young, D. & Cole, S. The catalase–peroxidase gene and isoniazid resistance of *Mycobacterium tuberculosis*. *Nature* **358**, 591–593 (1992).
23. Santangelo, M. P. et al. Negative transcriptional regulation of the *mce3* operon in *Mycobacterium tuberculosis*. *Microbiology* **148**, 2997–3006 (2002).
24. Santangelo, M. P. et al. Study of the role of Mce3R on the transcription of *mce* genes of *Mycobacterium tuberculosis*. *BMC Microbiol.* **8**, 38 (2008).
25. De la Paz Santangelo, M. et al. Mce3R, a TetR-type transcriptional repressor, controls the expression of a regulon involved in lipid metabolism in *Mycobacterium tuberculosis*. *Microbiology* **155**, 2245–2255 (2009).
26. Karakousis, P. C., Williams, E. P. & Bishai, W. R. Altered expression of isoniazid-regulated genes in drug-treated dormant *Mycobacterium tuberculosis*. *J. Antimicrob. Chemother.* **61**, 323–331 (2008).
27. Vilcheze, C. et al. Enhanced respiration prevents drug tolerance and drug resistance in *Mycobacterium tuberculosis*. *Proc. Natl Acad. Sci. USA* **114**, 4495–4500 (2017).
28. Schoutrop, E. L. M. et al. The stability of antimycobacterial drugs in media used for drug susceptibility testing. *Diagn. Microbiol. Infect. Dis.* **92**, 305–308 (2018).
29. Rouse, D. A., DeVito, J. A., Li, Z., Byer, H. & Morris, S. L. Site-directed mutagenesis of the *katG* gene of *Mycobacterium tuberculosis*: effects on catalase–peroxidase activities and isoniazid resistance. *Mol. Microbiol.* **22**, 583–592 (1996).
30. Liu, Y. et al. Immune activation of the host cell induces drug tolerance in *Mycobacterium tuberculosis* both in vitro and in vivo. *J. Exp. Med.* **213**, 809–825 (2016).
31. Ma, S. et al. Integrated modeling of gene regulatory and metabolic networks in *Mycobacterium tuberculosis*. *PLoS Comput. Biol.* **11**, e1004543 (2015).
32. Mawuenyega, K. G. et al. *Mycobacterium tuberculosis* functional network analysis by global subcellular protein profiling. *Mol. Biol. Cell* **16**, 396–404 (2005).
33. Raimunda, D., Long, J. E., Padilla-Benavides, T., Sassetti, C. M. & Arguello, J. M. Differential roles for the Co^{2+}/Ni^{2+} transporting ATPases, CtpD and CtpJ, in *Mycobacterium tuberculosis* virulence. *Mol. Microbiol.* **91**, 185–197 (2014).
34. Lew, J. M., Kapopoulou, A., Jones, L. M. & Cole, S. T. TubercuList—10 years after. *Tuberculosis (Edinb.)* **91**, 1–7 (2011).
35. Patel, S. J. et al. Fine-tuning of substrate affinity leads to alternative roles of *Mycobacterium tuberculosis* Fe^{2+}-ATPases. *J. Biol. Chem.* **291**, 11529–11539 (2016).
36. Bulatovic, V. M. et al. Oxidative stress increases susceptibility of *Mycobacterium tuberculosis* to isoniazid. *Antimicrob. Agents Chemother.* **46**, 2765–2771 (2002).
37. Slayden, R. A. & Barry, C. E. 3rd. The genetics and biochemistry of isoniazid resistance in *Mycobacterium tuberculosis*. *Microbes Infect.* **2**, 659–669 (2000).

38. Kohanski, M. A., Dwyer, D. J., Hayete, B., Lawrence, C. A. & Collins, J. J. A common mechanism of cellular death induced by bactericidal antibiotics. *Cell* **130**, 797–810 (2007).
39. Hu, J., Zhao, L. & Yang, M. A GntR family transcription factor positively regulates mycobacterial isoniazid resistance by controlling the expression of a putative permease. *BMC Microbiol.* **15**, 214 (2015).
40. Zhou, L., He, Z. G. & Li, W. AraR, an L-arabinose-responding transcription factor, negatively regulates resistance of *Mycobacterium smegmatis* to isoniazid. *Biochem. (Mosc.)* **84**, 540–552 (2019).
41. Ehrt, S. et al. Controlling gene expression in mycobacteria with anhydrotetracycline and Tet repressor. *Nucleic Acids Res.* **33**, e21 (2005).
42. Ehrt, S. & Schnappinger, D. Controlling gene expression in mycobacteria. *Future Microbiol.* **1**, 177–184 (2006).
43. Guo, M. et al. Dissecting transcription regulatory pathways through a new bacterial one-hybrid reporter system. *Genome Res.* **19**, 1301–1308 (2009).
44. Klotzsche, M., Ehrt, S. & Schnappinger, D. Improved tetracycline repressors for gene silencing in mycobacteria. *Nucleic Acids Res.* **37**, 1778–1788 (2009).
45. *BEI Resources* (American Type Culture Collection, 2020); www.beiresources.org
46. Rock, J. M. et al. Programmable transcriptional repression in mycobacteria using an orthogonal CRISPR interference platform. *Nat. Microbiol.* **2**, 16274 (2017).
47. Langmead, B. & Salzberg, S. L. Fast gapped-read alignment with Bowtie 2. *Nat. Methods* **9**, 357–359 (2012).
48. Li, H. et al. The Sequence Alignment/Map format and SAMtools. *Bioinformatics* **25**, 2078–2079 (2009).
49. Ma, S. et al. Transcriptomic signatures predict regulators of drug synergy and clinical regimen efficacy against tuberculosis. *mBio* **10**, e02627-19 (2019).
50. Rustad, T. R., Harrell, M. I., Liao, R. & Sherman, D. R. The enduring hypoxic response of *Mycobacterium tuberculosis*. *PLoS ONE* **3**, e1502 (2008).
51. Nandakumar, M., Prosser, G. A., De Carvalho, L. P. & Rhee, K. Metabolomics of *Mycobacterium tuberculosis*. *Methods Mol. Biol.* **1285**, 105–115 (2015).
52. Garcia, B. J., Datta, G., Davidson, R. M. & Strong, M. MycoBASE: expanding the functional annotation coverage of mycobacterial genomes. *BMC Genomics* **16**, 1102 (2015).
53. Mi, H. et al. PANTHER version 11: expanded annotation data from Gene Ontology and Reactome pathways, and data analysis tool enhancements. *Nucleic Acids Res.* **45**, D183–D189 (2017).

Acknowledgements

We gratefully acknowledge J. Rock for kindly providing us with the pJR965 plasmid encoding a tetracyline-inducible dCas9 and kanamycin-selectable marker. We also thank J. Winkler, J. Lohmiller and R. Liao for technical assistance and S. Shen for helpful discussions. This work was supported by the National Institutes of Health (grant nos. U19 AI106761; U19 AI111276; U19 AI135976 and 5T32AI007509).

Author contributions

S.M., T.R.R. and D.R.S. conceived of the study, led the design, generated data, analysed the results and drafted the manuscript. R.M. developed the software to convert raw sequencing data into abundance values for each TFI strain. S.J.H. generated data and assembled the pooled TFI library cultures. J.F.-J. assisted with sample preparation for sequencing. V.S. and K.Y.R. generated, analysed and interpreted the metabolite profiling data. A.F., N.F. and C.G. generated the CRISPRi strain.

Competing interests

The authors declare no competing interests.

Additional information

Extended data is available for this paper at https://doi.org/10.1038/s41564-020-00810-x.

Supplementary information is available for this paper at https://doi.org/10.1038/s41564-020-00810-x.

Correspondence and requests for materials should be addressed to D.R.S.

Reprints and permissions information is available at www.nature.com/reprints.

Publisher's note Springer Nature remains neutral with regard to jurisdictional claims in published maps and institutional affiliations.

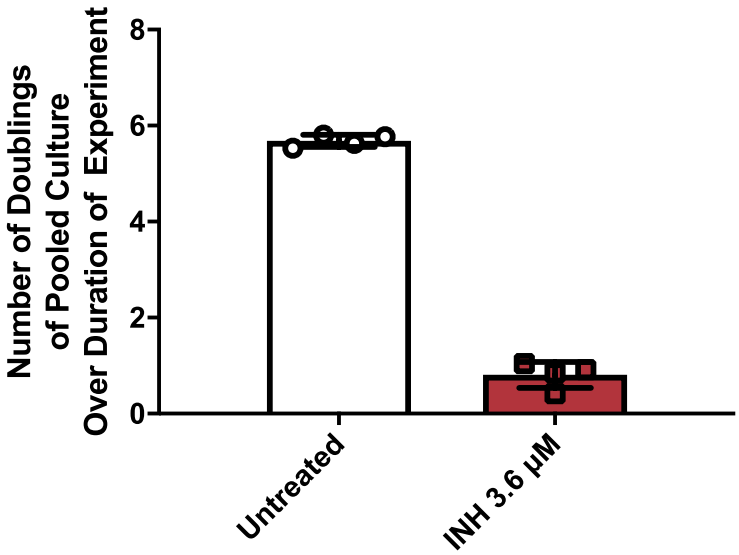

Extended Data Fig. 1 | Comparing TFI pool growth between experimental conditions. Number of doublings for TFI strain pool over duration of TRIP experiments in the untreated vs. INH treated conditions, estimated from the change of OD600 over the course of the experiment. Data show mean ± SD of four biological replicates from a representative experiment (three independent experiments were performed in total).

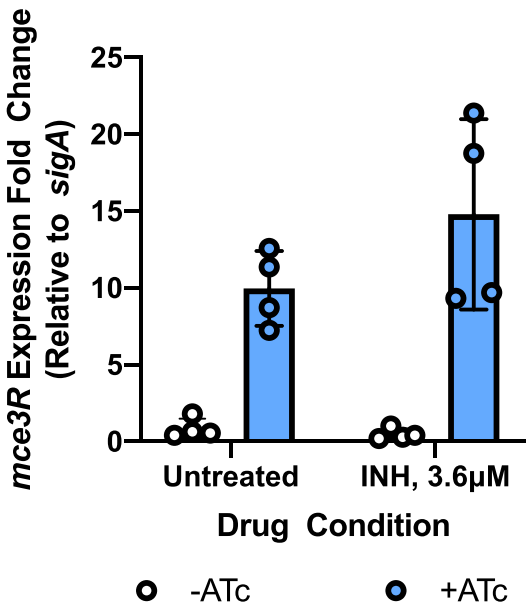

Extended Data Fig. 2 | Chemical induction triggers *mce3R* expression change. Expression fold change of *mce3R* relative to the housekeeping gene *sigA*, assessed by qPCR. Data show mean ± SD of 4 biological replicates from a representative experiment (two were performed in total). Conditions compared are in absence (white bars) and presence (black bars) of anhydrous-tetracycline (ATc) inducer, and presence and absence of INH exposure. Results show at least 8-fold activation of *mce3R* expression upon induction with ATc in both absence and presence of INH ($p = 0.00035$, two-sided t-test for -ATc untreated vs. +ATc untreated; $p = 0.0036$, two-sided t-test for -ATc + INH vs. +ATc + INH).

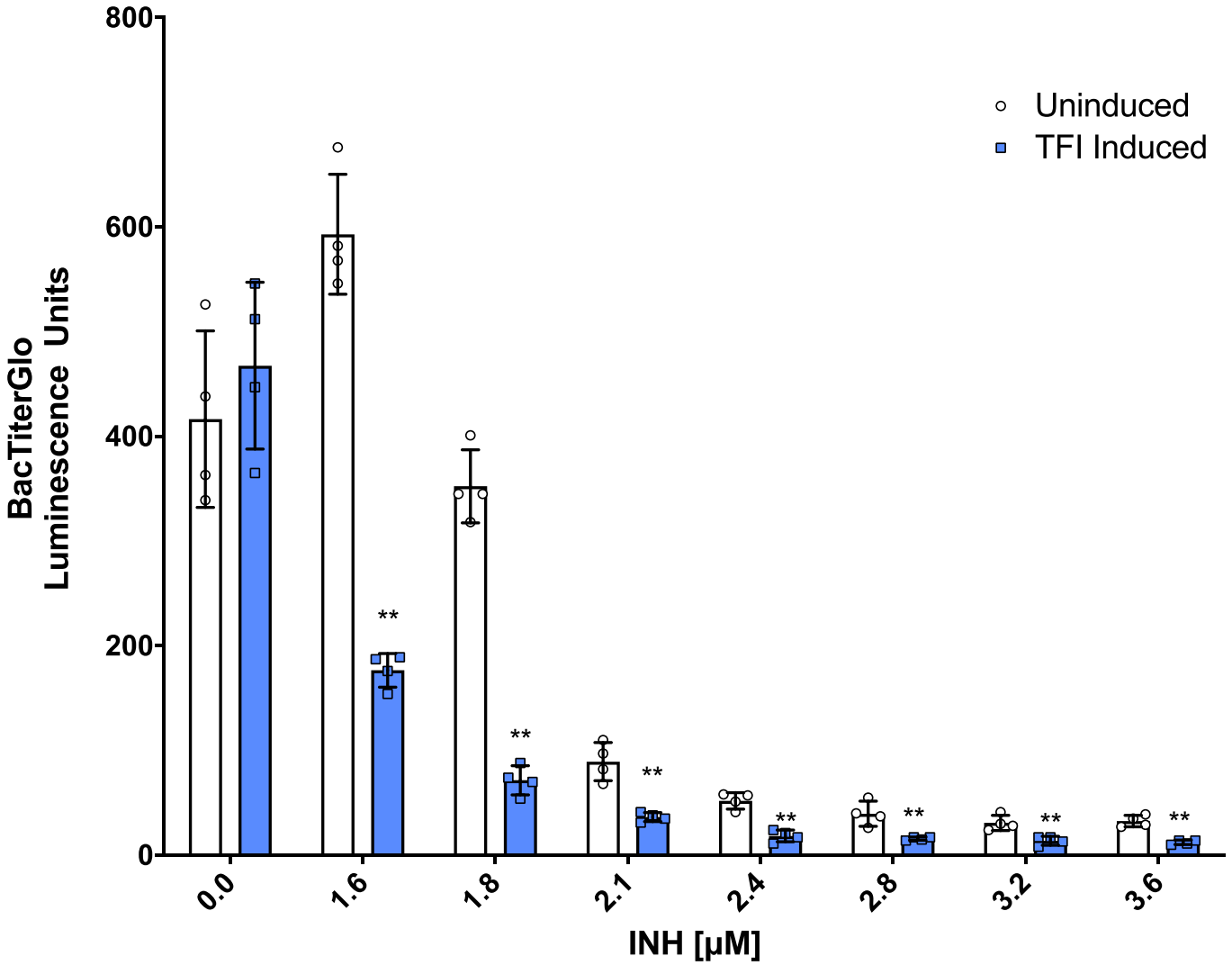

Extended Data Fig. 3 | *mce3R*$_{ind}$ metabolic viability after 7 days INH. Viability upon TFI induction (blue) is compared to uninduced (white), as measured by luminescence (see Methods). Data presented as mean Error bars show ± SD from four biological replicates. ** indicates significant differences between induction states ($p = 8.3 \times 10^{-6}$ comparing uninduced vs. TFI induced at 1.6 μM; $p = 5.7 \times 10^{-6}$ comparing uninduced vs. TFI induced at 1.8 μM; $p = 1.3 \times 10^{-3}$ comparing uninduced vs. TFI induced at 2.1 μM; $p = 4.3 \times 10^{-4}$ comparing uninduced vs. TFI induced at 2.4 μM; $p = 7.6 \times 10^{-3}$ comparing uninduced vs. TFI induced at 2.8 μM; $p = 6.9 \times 10^{-3}$ comparing uninduced vs. TFI induced at 3.2 μM; $p = 4.6 \times 10^{-4}$ comparing uninduced vs. TFI induced at 3.6 μM). Each p-value was calculated based on a two-sided t-test.

A

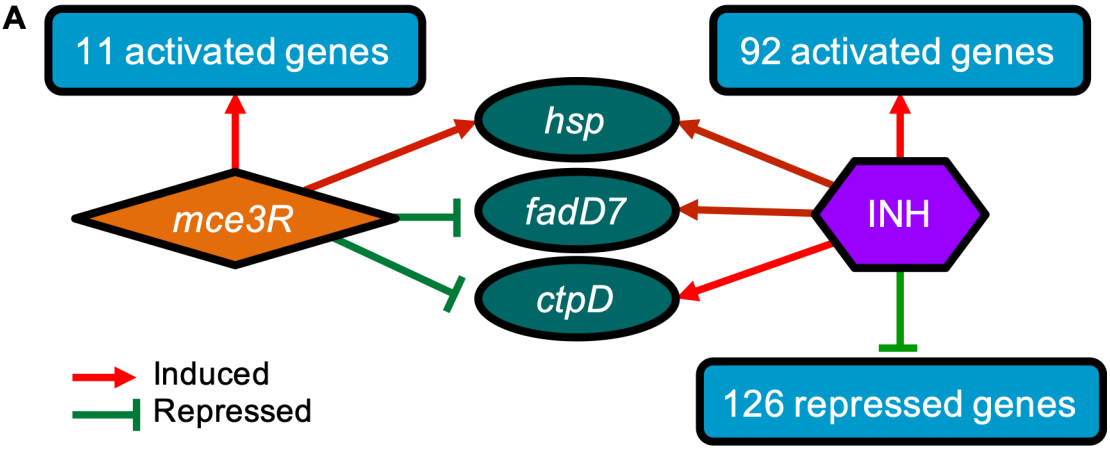

B

Target Genes	INH response log2 fold-change	*mce3R* induction response log2 fold-change
fadD7	0.88	-1.14
hsp	1	1.28
ctpD	1.99	-1.09

Extended Data Fig. 4 | Overlap of genes regulated by *mce3R* that also modulate expression in baseline response to INH exposure. a, Network diagram depicts the genes differentially expressed upon induction of *mce3R* expression (left), and upon exposure to INH (right). Three genes alter expression under both these conditions. **b**, Table summarizes the expression fold-changes of the genes perturbed both by *mce3R* induction and INH exposure.

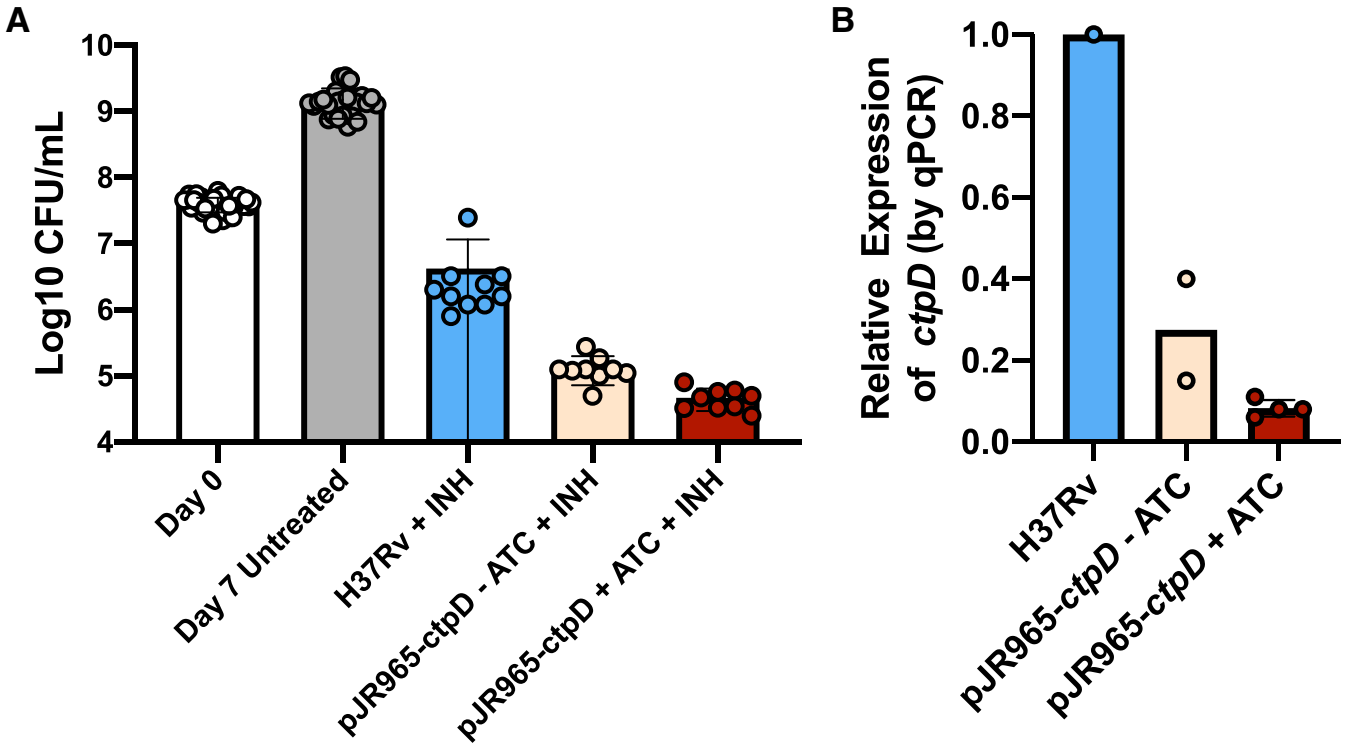

Extended Data Fig. 5 | Association between *ctpD* expression and INH sensitivity. a, CFU/mL at 0 days and 7 days of H37Rv (black bar) and a *ctpD* CRISPRi-knockdown strain without (yellow) and with (red) chemical induction of CRISPRi activity. Both strains were exposed to 3.6 μM INH or no drug. There was no significant difference between the growth of strains without drug, and the average untreated CFU/mL is plotted in the gray bar. Data show mean ± SD of three biological replicates from two independent experiments (for H37Rv conditions) or one experiment (pJR965-*ctpD* conditions). There is a significant difference between the CRISPRi knockdown and wildtype strains ($p = 0.00027$ for Day 7 H37Rv + INH vs. Day 7 pJR965-*ctpD* – ATc + INH, Wilcoxon ranksum test with continuity correction; $p = 0.00027$ for Day 7 H37Rv + INH vs. Day 7 pJR965-*ctpD* + ATc + INH, Wilcoxon ranksum test with continuity correction; $p = 0.0012$ for Day 7 pJR965-*ctpD* – ATc + INH vs. Day 7 pJR965-*ctpD* + ATc + INH, Wilcoxon ranksum test with continuity correction). **b**, qPCR quantification of *ctpD* expression levels relative to the wildtype H37Rv in the CRISPRi knockdown strain with and without chemical induction of activity. The CRISPRi strain exhibited marked repression even in the absence of chemical induction. Data shown are from two biological replicates for the CRISPRi knockdown strain, uninduced and four biological replicates for the CRISPRi knockdown strain with induction. The experiment was performed once.

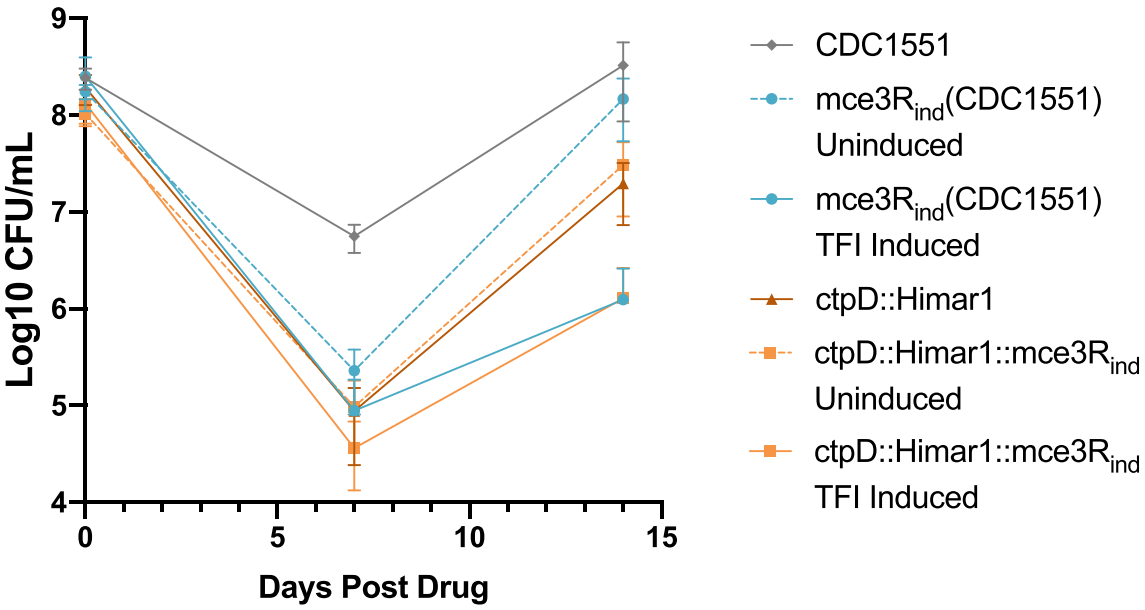

Extended Data Fig. 6 | Comparing the effect of *in vitro* INH on *mce3R* and *ctpD* perturbation strains. We measured the effect of *mce3R* induction in the CDC1551 strain background (blue) and in the *ctpD*::Himar1 strain background (orange) on Mtb survival in INH (3.6 μM), added on Day 0, as quantified by CFU/mL. Solid blue and orange lines indicate TFI induction and dashed blue and orange lines indicate TFI uninduced. As additional controls, we also compared survival of the CDC1551 wildtype strain (gray), as well as the *ctpD*::Himar1 strain (red). The data suggest that *mce3R* induction conveys significant additional fitness defect relative to *ctpD*::Himar1 strain at day 14 ($p = 0.00058$, two-sided t-test comparing *ctpD*::Himar1:: *mce3R*$_{ind}$ TFI induced vs. *ctpD*::Himar1; $p = 0.0024$, two-sided t-test comparing *mce3R*$_{ind}$ (CDC1551) TFI induced vs. CDC1551). There appears to be a modest (though not statistically significant) difference in the extent of INH-mediated killing at 7 days between the *ctpD*::Himar strain (red) and the *ctpD*::Himar1 strain with *mce3R* induction (orange solid) ($p = 0.09$, two-sided t-test). Data show mean ± SD of three biological replicates from one experiment.

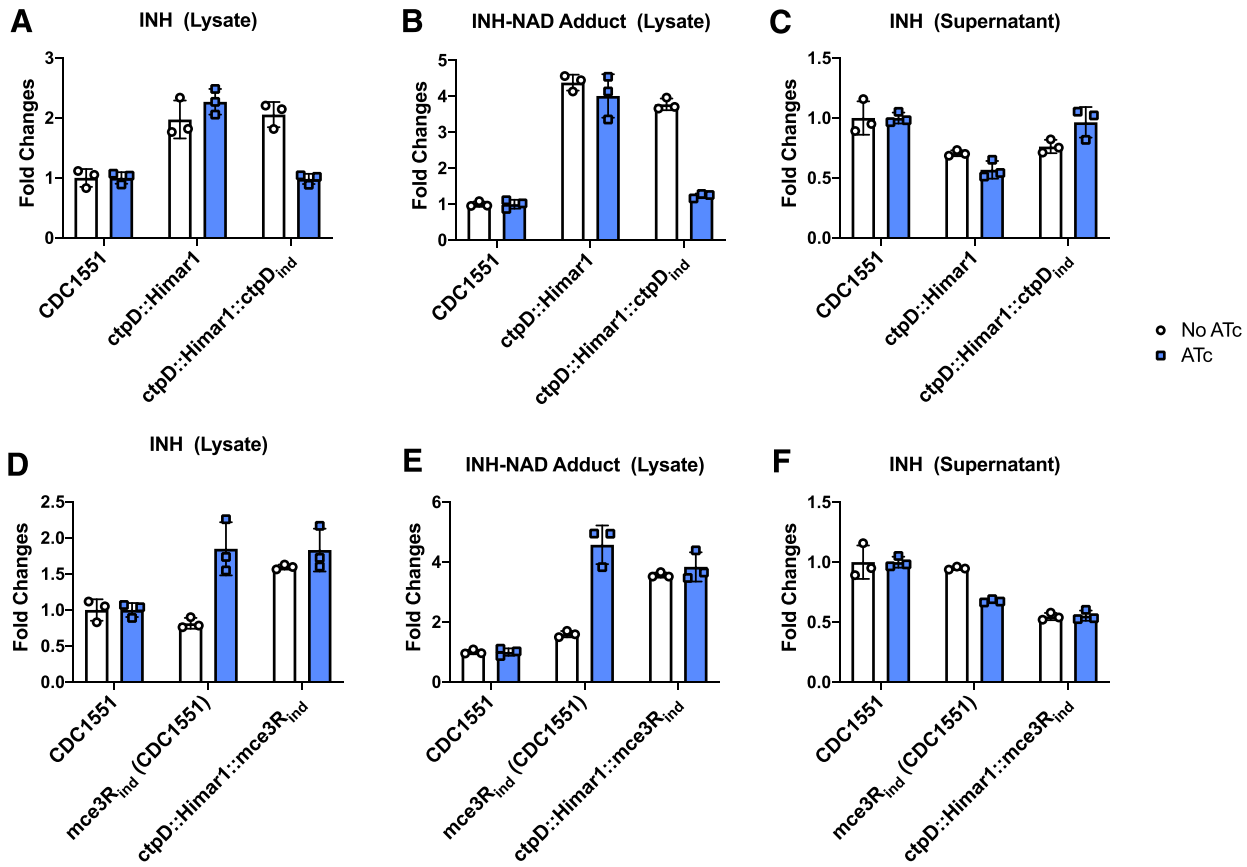

Extended Data Fig. 7 | Association between *mce3R*, *ctpD* expression and abundance of INH and INH-NAD adduct during drug exposure. Relative abundance of INH and INH-NAD adduct in Mtb lysate (panels **a**, **b**, **d**, **e**, or supernatant (panels **c**, **f**) of strains exposed to 7.2μM INH for 24 hours. Panels **a**, **b**, and **c** show effect of *ctpD* transposon disruption and complementation with episomally ATc-inducible *ctpD* expression. Panels **d**, **e**, and **f** show the effect of *mce3R* induction with or without *ctpD* transposon disruption. *ctpD* disruption conveyed increased intracellular INH and INH-NAD levels and concomitant decreased levels of INH in the supernatant. Induction of *mce3R* also increases intracellular INH and INH-NAD levels, but does not convey additional accumulation increase in the *ctpD* transposon strain background. Bars plot mean ± SD for 3 biological replicates.

nature research

Corresponding author(s): David R. Sherman

Last updated by author(s): Sep 11, 2020

Reporting Summary

Nature Research wishes to improve the reproducibility of the work that we publish. This form provides structure for consistency and transparency in reporting. For further information on Nature Research policies, see our Editorial Policies and the Editorial Policy Checklist.

Statistics

For all statistical analyses, confirm that the following items are present in the figure legend, table legend, main text, or Methods section.

n/a	Confirmed	
☐	☒	The exact sample size (*n*) for each experimental group/condition, given as a discrete number and unit of measurement
☐	☒	A statement on whether measurements were taken from distinct samples or whether the same sample was measured repeatedly
☐	☒	The statistical test(s) used AND whether they are one- or two-sided *Only common tests should be described solely by name; describe more complex techniques in the Methods section.*
☐	☒	A description of all covariates tested
☐	☒	A description of any assumptions or corrections, such as tests of normality and adjustment for multiple comparisons
☐	☒	A full description of the statistical parameters including central tendency (e.g. means) or other basic estimates (e.g. regression coefficient) AND variation (e.g. standard deviation) or associated estimates of uncertainty (e.g. confidence intervals)
☐	☒	For null hypothesis testing, the test statistic (e.g. *F*, *t*, *r*) with confidence intervals, effect sizes, degrees of freedom and *P* value noted *Give P values as exact values whenever suitable.*
☐	☒	For Bayesian analysis, information on the choice of priors and Markov chain Monte Carlo settings
☐	☒	For hierarchical and complex designs, identification of the appropriate level for tests and full reporting of outcomes
☐	☒	Estimates of effect sizes (e.g. Cohen's *d*, Pearson's *r*), indicating how they were calculated

Our web collection on statistics for biologists contains articles on many of the points above.

Software and code

Policy information about availability of computer code

Data collection	Next generation sequencing for TRIP was performed at the University of Washington Northwest Genomics Center with the Illumina NextSeq 500 Mid Output v2 Kit (Illumina Inc, San Diego, CA). Next generation sequencing for RNAseq was performed at the University of Washington Northwest Genomics Center with the Illumina NextSeq 500 High Output v2 Kit (Illumina Inc, San Diego, CA).
Data analysis	Read alignment for both TRIP and RNAseq was carried out using a custom processing pipeline that harnesses the Bowtie 2 utilities. To assess relative abundance of each barcoded transcription factor induction strain, we implemented a custom analysis pipeline in R (version 3.3.0). Gene Ontology enrichment analysis was performed with a custom pipeline implemented in Matlab (version R2013a). Code for all of the aforementioned pipelines are available at: https://github.com/DavidRShermanLab/TRIPscreen, https://github.com/robertdouglasmorrison/DuffyNGS, and https://github.com/robertdouglasmorrison/DuffyTools.

For manuscripts utilizing custom algorithms or software that are central to the research but not yet described in published literature, software must be made available to editors and reviewers. We strongly encourage code deposition in a community repository (e.g. GitHub). See the Nature Research guidelines for submitting code & software for further information.

Data

Policy information about availability of data

All manuscripts must include a data availability statement. This statement should provide the following information, where applicable:

- Accession codes, unique identifiers, or web links for publicly available datasets
- A list of figures that have associated raw data
- A description of any restrictions on data availability

The data reported in the paper are available in the Supplementary Materials. The raw .fastq sequence data files for the TRIP experiments are deposited in the Sequence Read Archive database [PRJNA483505]. The RNAseq data are deposited in the Gene Expression Omnibus database [GSE151991]. The code required to process the sequenced reads are available at: https://github.com/robertdouglasmorrison/DuffyNGS, https://github.com/robertdouglasmorrison/DuffyTools, and https://github.com/DavidRShermanLab/TRIPscreen.

Field-specific reporting

Please select the one below that is the best fit for your research. If you are not sure, read the appropriate sections before making your selection.

☒ Life sciences ☐ Behavioural & social sciences ☐ Ecological, evolutionary & environmental sciences

For a reference copy of the document with all sections, see nature.com/documents/nr-reporting-summary-flat.pdf

Life sciences study design

All studies must disclose on these points even when the disclosure is negative.

Sample size	We elected to use at three biological replicates for experiments, where possible, in order to ensure the ability to detect a 2-fold change with > 0.95 power at a 5% false positive rate.
Data exclusions	TRIP screen samples that generated sequencing libraries with fewer than 10,000 valid read pairs were excluded from analysis to ensure sufficient read depth coverage of each of the strain-specific barcodes.
Replication	Each TRIP experiment included four biological replicates, and experiments were performed twice. The replicates were consistent across experiments. Each follow-up experiment involving validation with individual mutant strains was performed two or three times, with 3 biological replicates per condition. The results replicated across experiments.
Randomization	Each biological replicate in a TRIP screen or drug exposure experiment was a culture that was inoculated by sampling randomly from an individual starting culture.
Blinding	The sample library preparation for sequencing and the data processing of the sequencing data were blinded.

Reporting for specific materials, systems and methods

We require information from authors about some types of materials, experimental systems and methods used in many studies. Here, indicate whether each material, system or method listed is relevant to your study. If you are not sure if a list item applies to your research, read the appropriate section before selecting a response.

Materials & experimental systems

n/a	Involved in the study
☒	☐ Antibodies
☒	☐ Eukaryotic cell lines
☒	☐ Palaeontology and archaeology
☒	☐ Animals and other organisms
☒	☐ Human research participants
☒	☐ Clinical data
☐	☒ Dual use research of concern

Methods

n/a	Involved in the study
☒	☐ ChIP-seq
☒	☐ Flow cytometry
☒	☐ MRI-based neuroimaging

Dual use research of concern

Policy information about dual use research of concern

Hazards

Could the accidental, deliberate or reckless misuse of agents or technologies generated in the work, or the application of information presented in the manuscript, pose a threat to:

No	Yes	
☐	☒	Public health
☒	☐	National security
☒	☐	Crops and/or livestock
☒	☐	Ecosystems
☒	☐	Any other significant area

Hazards: any accidental, deliberate, or reckless misuse of Mycobacterium tuberculosis (the pathogen responsible for the greatest loss of human life worldwide) has the potential to pose a threat to public health.

For examples of agents subject to oversight, see the United States Government Policy for Institutional Oversight of Life Sciences Dual Use Research of Concern.

Experiments of concern

Does the work involve any of these experiments of concern:

No	Yes	
☒	☐	Demonstrate how to render a vaccine ineffective
☐	☒	Confer resistance to therapeutically useful antibiotics or antiviral agents
☒	☐	Enhance the virulence of a pathogen or render a nonpathogen virulent
☒	☐	Increase transmissibility of a pathogen
☒	☐	Alter the host range of a pathogen
☒	☐	Enable evasion of diagnostic/detection modalities
☒	☐	Enable the weaponization of a biological agent or toxin
☒	☐	Any other potentially harmful combination of experiments and agents

Precautions and benefits

Biosecurity precautions: All experiments with Mycobacterium tuberculosis (Mtb) were conducted in specialized biosafety level 3 (BSL-3) facilities designed and equipped to ensure biocontainment and biosafety. Entry to the facilities is cardkey controlled. The labs have negative pressure, a controlled-access anteroom, and procedures in place to safely acquire, process, ship, and store biologically hazardous specimens that contain Mtb and other infectious agents. All work with live bacteria is conducted within type II biosafety cabinets, and users are required to use BSL-3 level-appropriate personal protective equipment (PPE) while in the facility. The facility has a faculty-level director who oversees user access, and the facility is managed by a dedicated manager with >15 years of experience with Mtb.

Biosecurity oversight: Use of Mycobacterium tuberculosis (Mtb) and other BSL3 organisms is reviewed by the Research Environmental Health and Safety Office and/or the Institutional Biosafety Committee. All laboratory personnel complete institutional biosafety training, laboratory specific training and instruction in good microbiologic practices prior to performing working with BSL-3 organisms.

Benefits: The approach described in this study has the potential to uncover additional Mycobacterium tuberculosis (Mtb) intervention targets, and lead to biological insights that inform treatment strategies that are more effective and could shorten the necessary duration of treatment. Together these insights could contribute to policy changes that might save lives.

Communication benefits: The approach described in this study has the potential to uncover additional Mycobacterium tuberculosis (Mtb) intervention targets, and lead to biological insights that inform treatment strategies that are more effective and could shorten the necessary duration of treatment. There are many potential applications for the approach described in the study that are beyond the scope of a single laboratory to tackle. Moreover, the underlying strategy of regulatory-centric genetic screening could be adapted for other organisms. Therefore, communication of these results will amplify the potential beneficial impacts of this work.